Generation and Thermal Simulation of a Digital Model of the Female Breast in Prone Position

Jose-Luis Gonzalez-Hernandez

Department of Mechanical Engineering, Rochester Institute of Technology 76 Lomb Memorial Drive, Rochester, NY-14623, USA jxg4140@rit.edu
ASME Student Member

Satish G. Kandlikar*

Department of Mechanical Engineering, Rochester Institute of Technology 76 Lomb Memorial Drive, Rochester, NY-14623, USA sgkeme@rit.edu
ASME Fellow

Donnette Dabydeen

Department of Radiology, Rochester General Hospital 1425 Portland Avenue, Rochester, NY-14621, USA Donnette.Dabydeen@rochesterregional.org

Lori Medeiros

Rochester General Breast Center 1425 Portland Avenue, Rochester, NY-14621, USA Lori.Medeiros@rochesterregional.org

Pradyumna Phatak

Department of Medicine and Lipson Cancer Institute, Rochester General Hospital 1425 Portland Avenue, Rochester, NY-14621, USA Pradyumna.Phatak@rochesterregional.org

*Corresponding author

Satish G. Kandlikar sgkeme@rit.edu

Department of Mechanical Engineering, Rochester Institute of Technology, 76 Lomb Memorial Drive, Rochester, NY-14623, USA

Telephone: +1 585-475-6728

Fax: +1 585-475-6879

ABSTRACT

Infrared breast thermography has been associated with the early detection of breast cancer. However, findings in previous studies have been inconclusive. The upright position of subjects during imaging introduces errors in interpretation because it blocks the optical access in the inframammary fold region and alters the temperature due to contact between breast and chest wall. These errors can be avoided by imaging breasts in prone position. Although the numerical simulations provide insight into thermal characteristics of the female breast with a tumor, most simulations in the past have used cubical and hemispherical breast models. We hypothesize that a breast model with the actual breast shape will provide true thermal characteristics that are useful in tumor detection. A digital breast model in prone position is developed to generate the surface temperature profiles for breasts with tumors. The digital breast model is generated from sequential MRI images and simulations are performed using Finite Volume Method employing Pennes bioheat equation. We investigated the effect of varying the tumor metabolic activity on the surface temperature profile. We compared the surface temperature profile for various tumor metabolic activities with a case without tumor. The resulting surface temperature rise near the location of the tumor was between 0.665 and 1.023 °C, detectable using modern Infrared cameras. This is the first time that numerical simulations are conducted in a model with the actual breast shape in prone position to study the surface temperature changes induced by breast cancer.

Key words: Breast thermography, digital breast model, detection of breast cancer, actual breast shape, numerical simulation of the breast

1. - INTRODUCTION

Breast cancer (BC) is the most common form of cancer among women in the US, with more than 246,000 new cases diagnosed in 2016. It is estimated that one in every eight women (12.5%) will develop BC during her lifetime [1] and that one in every 24 woman (4.16%) will die of BC [2]. Early detection of BC is crucial to increase the survival of individuals; since 2003, the mortality rate has dropped ~ 1.2% annually mainly due to improvements in detection and treatment [1]. Therefore, improving available BC screening techniques is necessary for more accurate early detection.

1.1 – SCREENING OF BREAST CANCER

Manual self-examination is recommended monthly by the America Medical Association. A self-breast exam consists of palpating the breasts with the fingers moving

in various patterns to detect abnormal lumps. Although self-exams can detect up to 50 % of asymptomatic BCs [3], it is highly individual-dependent and results in a high rate of false positives (~50%), which can cause anxiety [4].

Various clinical screening techniques such as mammography, ultrasound and Magnetic Resonance Imaging (MRI) are widely used for BC screening. Mammography consists of emitting low energy X-rays to the breasts while they are compressed between two plates to detect abnormal masses and calcifications. It has been the most prevalent technique since the early 60's and is recommended every 1 to 2 years for women aged 40 or older [5], [6]. The sensitivity of mammography decreases in women with dense breasts (found in > 40% of women) because dense tissue can mask tumors resulting in high false negative rates. Digital Breast Tomosynthesis or 3D mammography has been shown to improve the detection of BC. However, it suffers from subject discomfort, higher cost and increased radiation exposure as compared to mammography [7].

Ultrasound or sonography is one of the most commonly used adjuncts for breast cancer screening. It involves high frequency sound waves directed to the breasts through a transducer. The success of this modality depends on the experience of the operator and findings may be difficult to reproduce. Despite its low cost, it results in both high false positives and high false negatives. MRI uses strong magnetic fields and radio waves to generate images of the breasts. Supplemental screening with contrast-enhanced breast MRI is recommended in women at high risk for breast cancer. However, MRI is time consuming, expensive and results in a large number of false positives [8].

1.2 - BREAST THERMOGRAPHY

Infrared thermography uses infrared radiation emitted by an object to measure its temperature. Since every object emits thermal radiation, the temperature of the object can be related to its output on the electromagnetic spectrum. For example, objects that have a temperature over 500 K will emit radiation in the visible spectrum. At human body temperatures, infrared radiations are emitted in the wavelengths bands of 2-20 µm [9]. Human bodies are often represented as a blackbody because their emissivity is \sim 0.97 (Watmough and Oliver [10]) with negligible variations for different skin colors. A blackbody is defined as an object that absorbs all electromagnetic radiation, and whose absorption of radiation is related to its emission according with Planck's Radiation Law [11]. Integrating Plank's Radiation Law for all frequencies, the Stefan-Boltzman law is obtained, which describes the emissive power from a black body. For a real surface with emissivity ϵ , Stefan-Boltzman is [11]:

$$E = \epsilon \sigma T^4 \tag{1}$$

Therefore, the wavelength of infrared radiation can be related to the temperature of human skin. Further details of the methodology are given by Lahiri et al [9].

Infrared (IR) breast thermography is an FDA approved adjunct modality for BC screening. In this technique, the surface temperature of the breasts is acquired by an IR camera. In individuals without breast cancer, the temperature distribution of the breasts is close to symmetric. When cancer is present, the symmetry is lost because the temperature of the breast with cancer is affected by two factors: (1) tumors have a higher metabolic activity than the surrounding healthy tissue, and (2) tumors are associated with Satish G. Kandlikar

formation of new blood vessels (angiogenesis) to sustain their accelerated growth and develop a more robust vascular network [12]. The temperature rise caused by the presence of tumors has been measured to be up to 3.5 °C as compared to the contralateral breast [13]. The ensuing surface thermal changes depend on the location of the tumor in the breast, its metabolic activity and vascularity, which are related to grade and histology of the tumor [12], [13]. IR breast thermography has been associated with the detection of pre-invasive lesions [14] and with the early detection of BC [15]. Effectiveness of IR thermography has been however limited. The dynamic IR thermography, which involves cooling the breasts prior to imaging, has been proposed to improve the performance by enhancing the thermal contrast caused by tumors; however its advantage over steady state thermography remains unclear [16]. Conventional IR examinations are conducted while patients are upright. In this position the chest wall contacts the inframammary fold of the breasts, which creates thermal artifacts [17].

One of the difficulties with current IR imaging systems is that they do not directly provide definitive information on the location and size of the tumors within the breast. Such information is available through MRI images of the breast. To make the simulation and detection seamless, the digital breast model can be generated using the MRI images; this allows for exact positioning of the tumor in the model.

This paper presents a new approach to predict the surface temperature distribution of a breast with and without tumor through numerical simulations. The underlying digital model is created from sequential MRI images of the breast in prone position because this imaging modality allows to obtain the exact tumor location and size.

Such information is not available through the IR images, hence the use of MRI images becomes essential. Although there are techniques to obtain digital models with the actual shape while patients are upright [18], the exact tumor position within the breast cannot be obtained accurately.

Numerical simulations on a model with the breast shape in prone position are expected to provide accurate temperature predictions and a better understanding of the effect of tumor size and location on the resulting surface thermal profile of the breast.

2. - LITERATURE REVIEW

Biological tissues are a complex structure that comprises of fat, muscles, nerves, veins and arteries. The exact morphology of a tissue is unique to each individual and body part. To model a tissue, a set of assumptions must be made. The Pennes model or bioheat equation [19] is the most widely used model because information about the discrete vasculature is not needed. Pennes model assumes that the main heat exchange between blood vessels and surrounding tissue occurs at the wall of capillary vessels with a diameter between 5 and 150 μ m. Pennes model also accounts for the metabolic activity (heat generation) within tissues. This model provides accurate approximations for tissues with capillary vessels smaller than 300 μ m, such as those in the female breasts. Pennes model is given by:

$$\rho_t c_t \left(\frac{\partial T_t}{\partial t} \right) = \nabla \cdot (k_t \nabla T_t) + \omega_b c_b (T_a - T_t) + q_m \tag{2}$$

where ρ , c and k are the density, specific heat and thermal conductivity, respectively. The subscripts t, b and a refer to tissue, blood and arteries, respectively, ω is the blood perfusion rate per unit tissue volume in kg/m³-s and q_m is the metabolic activity within the tissue in W/m³. In the case of the breasts, the blood flow warms the surrounding tissue. Thus the temperature profile on a breast surface is influenced by heat conduction from chest wall, blood perfusion rate and tumor metabolic activity when cancer is present.

2.1 – MODELS OF THE FEMALE BREAST

Numerical simulations have also been used to aid in the estimation of tumor parameters through artificial intelligence algorithms [20] and have also aided the determination of unknown parameters through inverse modeling [21]. This modeling approach has the potential to improve the detection of breast cancer (BC) using IR thermography.

One of the first attempts to study the heat transfer processes on a female breast used a Cartesian model [22], [23]. Cartesian models have been used to study a portion of the female breast. These models can be either 2D or 3D sections of the breast with different layers of tissue. The bottom wall is considered to be at the core body temperature (37 °C) and the upper wall is considered as the surface of the breast, which is exposed to a convection boundary condition. The sides of the computational domain are considered adiabatic neglecting the heat flux across them. Tumors are embedded within the tissue along the centerline of the computational domain. Simulation of

Cartesian geometries provides insight into thermal interactions within the breasts. However, heat transfer processes in these models are close to unidimensional due to the boundary conditions, which do not provide an accurate description of the actual thermal profile.

Osman and Afify [24] developed a hemispherical domain with concentric tissue layers to study heat transfer in a breast without tumor. They considered a 144 mm diameter breast with four different layers of tissue, viz., core, muscle, fat and skin. They modified the Pennes equation to account for the countercurrent heat exchange between vessels. They also imposed values of perfusion rates that varied within the breast; this resulted in a warmer upper outer quadrant, which is in agreement with clinical thermograms. Later, Osman and Afify [25] modified their previous model to account for a tumor embedded within the breast; the tumor had a higher thermal conductivity, metabolic activity and perfusion rate than the healthy tissue. Their results showed that surface temperature variations can be observed in tumors with sizes ranging from 10 to 36 mm at depths from 5 to 18 mm. The hemispherical breast model developed by Osman and Afify have not been studied further mainly due to the complexity of its implementation. Further, the underlying assumptions of local variations in perfusion rate and counter current heat exchange are a matter of concern [26].

Sudharsan et al. [26] developed a hemispherical model with non-concentric layers to study the temperature variations induced by the presence of a tumor. They considered a 144 mm diameter breast with four different tissue layers named thoracic wall, muscle, gland and subcutaneous fat. Sudharsan and Ng [27], through a parametric study,

identified that tumor depth and metabolic activity are the parameters with the highest influence on surface temperature profile. Their results indicate that the environmental conditions that enhance the thermal contrast between the tumor and the surrounding healthy tissue are a high heat transfer coefficient and a low ambient temperature. Gonzalez [28] used a hemispherical breast model with two non-concentric layers, namely, the chest wall and the gland; in this model, the breast diameter was 180 mm. The author considered a spherical tumor embedded within the gland tissue; the perfusion rate and metabolic activity of the tumor were selected from [13]. The author conducted a parametric study to identify the minimum tumor size that can be detected at a given depth along the center axis for modern IR cameras with a thermal sensitivity of 20 mK. Their results indicate that tumors as deep as 70 mm can be found using steady state IR thermography. However, the value of the heat transfer coefficient was only 5 W/m²-K, in contrast with the values reported for clinical conditions of ~13 W/m²-K. Numerical models with non concentric layers have been used only for tumors along the centerline; yielding symmetric temperature distributions, which do not agree with clinical IR images.

More realistic breast models have been developed to accurately predict the temperature distribution over the breasts. Ng et al. [29], [30] developed a breast model capturing the breast outline from a mannequin with a breast size of 34 (cup C). The model consisted of five different layers consisting of muscle, core gland, fat gland, subcutaneous fat and nipple; the authors considered a tumor diameter of 32 mm. The temperatures predicted by their model show a colder nipple region and a warmer upper outer quadrant, in agreement with clinical thermograms. Jiang et al. [31], [32] developed a deformed

breast geometry from a hemispherical model with concentric layers to mimic individuals seated upright. They imposed a gravity load and the elastic deformation was estimated using finite element simulation. The authors reported that variation in tumor size has a smaller effect on the surface temperature profile than changing the tumor depth. They stated that the thermal contrast for tumors between 5 and 15 mm deep is higher than 0.5 °C; for tumors deeper than 20 mm, the thermal contrast reduces to less than 0.1 °C. Recently, Bezerra et al. [18] presented a methodology to generate 3D surrogate breast geometries by extracting curves of IR images in frontal and lateral views. The temperature predictions from these surrogate geometries, resemble the temperatures obtained during IR imaging. This model is useful in creating a 3D view of the thermal images generated using IR thermography.

Numerical models with a more accurate representation of the breast shape provide predictions that agree with thermal clinical data. However, the chest wall contacting the inframammary fold of the breast affects the temperature distribution. A numerical model with the actual breast shape in prone position is thus needed to understand the effect of various parameters on the surface temperature distribution on a position that avoids contact between the breasts and the chest wall.

3. – PROPOSED ANALYSIS METHODOLOGY

3.1 – GENERATION OF A DIGITAL MODEL OF THE FEMALE BREAST FROM MRI IMAGES

A digital model of the breast in prone position is developed using sequential MRI images. The images were provided by clinical collaborators at the Rochester General Satish G. Kandlikar

Hospital. The images do not contain any personal identifiers of the subjects. The digital model is then used to simulate the temperature distribution on the breast. The MRIs were captured at Rochester General Hospital using GE 3T MRI scanners. The MRI involved axial, coronal and sagittal imaging both pre and post contrast. The images were viewed and analyzed using PACS (Picture Archiving and Communication System) with the aid of iCAD VersaVue breast MRI Computer-Aided Detection software. They were viewed with both non-fat saturation and fat saturation. Although there is the potential of motion artifacts, the images were collected from the MRI tech and reimaged if blurry or if any movement was introduced.

Although the individual images have been refined by the internal software of the MRI machine, noise is still present. We have filtered the individual images in Matlab ® to reduce the noise and improve the edge detection process. We have used an image smoothing software (Autodesk Remake ®) and confirmed that the shape is smooth and actually reproduces the breast shape.

The steps to reconstruct the geometry of the breast from the sequential MRI images are described below (Figure 1):

- 1. Select a region of interest from the MRI images The model considers only one breast. In this step, the region containing the breast of interest is selected to ensure that only this region is analyzed and processed.
- 2. *Identify the tumor* In this step, the tumor is measured and its location is stored for future steps; the volume of the tumor is measured as well.

- 3. Filter the noise in the MRI images This step is necessary to reduce the noise present in the images and improve the edge detection process. In this step, a 3D median filter is applied. The dimensions of the applied 3D median filter are (3, 3, 3).
- 4. Detection of the outline of the breast For this step, a modified version of the Canny edge detector was used [33]. The algorithm employed detects a continuous outline of the breast. This is achieved by rejecting edges based on connectivity criteria and identifying missing edges that belong to the outline based on the continuity and connectivity of the edges.
- 5. Segmentation of the images The breast model considers only one type of tissue (two in the case of a breast with tumor). The region that lie within the outline of the breast is labeled as breast tissue and the region outside the outline is labeled as background.
- 6. Breast surface The breast surface was generated from the stack of MRI slices using the Marching Cubes algorithm [34], which results in a surface mesh composed of triangular elements. The resulting surface mesh is jagged and needs to be smoothed to represent more accurately the geometry of the breast.
- 7. Smoothing The surface mesh was smoothed using an algorithm that replaced the angle of a mesh face with the average angle of the neighboring faces [35]; it is similar to applying an averaging filter to a 3D image.
- 8. Finalizing geometry In the smoothed breast geometry, some regions of the mesh needed further smoothing. The software Autodesk Recap Photo was used for a final smoothing only on the regions that needed it. The resulting surface mesh is seamless and

accurate in its representation of the breast surface where the temperature profiles are numerically obtained.

Figure 2 shows the results of this approach using sequential MRI images. The generated geometry accurately resembles the geometry of the breasts, which will result in a more accurate model to predict the surface temperature distributions for comparison with the observed in clinical IR examinations in future work.

3.2 – NUMERICAL MODEL

For the computational domain, Pennes bioheat equation (2) is subjected to the following boundary conditions (Figure 3):

$$\frac{\partial T}{\partial n} = 0$$
 at the top, bottom and side faces (2)

$$T(x, y, z = 0) = T_c \tag{3}$$

$$-k\frac{\partial T}{\partial n} = h(T_S - T_{\infty})$$
 at the surface (4)

where n denotes the normal direction at a given location, T_c is the core body temperature, h is the heat transfer coefficient between the breast and the ambient temperature, T_s is the local temperature at the surface and T_∞ is the ambient temperature. These boundary conditions imply that heat is conducted from the chest at temperature T_c into the breast, and is convected at the breast surface.

Pennes model (2) lacks an analytical solution for the geometry of the breast and the boundary conditions used prompting the need for a numerical solution. To compute the numerical solution, the computational domain (breast model) must be separated into smaller volumes, known as mesh elements. The accuracy of the numerical solution Satish G. Kandlikar

depends greatly on the quality of the mesh employed. To solve Pennes bioheat equation subject to boundary conditions (2-4), a mesh in the computational domain with ~3.5 million elements is generated. The mesh is uniform throughout most of the domain, except towards the surface of the breast, where the mesh was finer to capture the temperature gradients accurately.

Once the mesh was created, the governing equations are discretized using the Finite Volume Method [36], which results in a set of simpler equations that can be solved using numerical techniques. A second order spatial discretization of the governing equation was used to improve the accuracy of the results.

In this work, the numerical solution is obtained using the software ANSYS Fluent. To take into consideration the two blood perfusion and metabolic activity terms in the Pennes bioheat equation, these terms were defined as source terms in the software using User Defined Functions (UDFs). The UDFs were prepared to vary the location and size of the tumor without need to again mesh the tumor domain separately. This offers flexibility if the position and size of the tumor is changed in the model because there is no need to re-mesh the domain; only the UDF will be modified to account for the new tumor position and size.

The UDFs are compiled in a parallel solver, which significantly reduces the computational time. The solution was considered satisfactory when the residuals of the Pennes bioheat equation were less than 1×10⁻¹⁶. This criterion was used because the temperature of the tissue in the previous iteration is used to compute the first source term (blood perfusion). After solving, the temperature of the tissue is updated and the

process repeats; therefore, the updated and previous temperatures must be very close to obtain accurate results. Table 1 lists the values of the thermophysical properties and environment conditions used in the simulations.

Gautherie [37] found a hyperbolic relation between the metabolic activity and the tumor doubling time. From this relation, he derived an expression for metabolic activity as a function of the tumor diameter. However, the accuracy of its predictions is about 50%. In another study, Ng and Sudharsan [27] conducted a parametric study of the effect of various parameters on the breast surface temperature caused by the presence of a tumor. The authors observed that the surface temperature is more sensitive to changes in metabolic activity of the tumor than to changes in the tumor diameter. Therefore, in this paper, for modelling purposes only, we consider a fixed tumor diameter with a varying metabolic activity. The modeling presented here is intended to show the effects of the parameters on the resulting surface temperature profiles. The authors agree that a more detailed parametric study is needed in future. Our work represents the first step in establishing a model that can be used in future simulations with the actual breast shape.

4. – RESULTS AND DISCUSSION

The digital model of the breast is used to predict the surface temperatures numerically. These simulations need to be compared with clinical data to verify the accuracy of the predictions. However, detailed temperature data correlated with tumor position and metabolic activity in prone position is lacking in the literature. In order to Satish G. Kandlikar

gain confidence in the numerical predictions, the numerical approach and the UDF developed will be validated by simulating a hemispherical breast model for which temperature measurements are available in the literature for an upright breast.

4.1 – VALIDATION OF THE UDF WITH EXPERIMENTAL DATA USING A HEMISPHERICAL BREAST MODEL

The UDF and the modeling approach are validated by using the experimental temperature distribution measured by Gautherie [37]. Gautherie introduced a needle thermocouple on a breast with a tumor to measure axially the internal temperature distribution. The thermophysical properties reported in the experiment are given in Table 1, except for the metabolic activity, which had a value of 29,000 W/m³ [37]. Gautherie reported a breast diameter of 18 cm, a tumor depth of 2 cm and a tumor diameter of 2.3 cm. As a hemispherical breast was modeled and the tumor was along the axis, only one quarter of a circle was simulated; an axisymmetric boundary condition along the axis was imposed. The results shown in Figure 4 demonstrate that the UDF developed can be used to accurately predict the temperature distribution within the female breast.

4.2 – SIMULATIONS ON THE DIGITAL BREAST MODEL GENERATED FROM MRI IMAGES

Numerical simulations are conducted using the reconstructed geometry of the breast from the MRI images using the validated UDFs. The diameter of the tumor was 2.9 cm. The tumor was located at 12 o' clock, at a depth of 4.5 cm, measured from the center of the tumor to the closest surface and the distance between the tumor and the chest

wall is 10 cm. A grid independence study has been prepared using a metabolic activity of $q_m = 29,000 \text{ W/m}^3$. Five different meshes were prepared to analyze the effect of number of elements in the solution. The number of elements for each mesh is shown in Table 2. The maximum surface temperature in the region surrounding the tumor is reported and used as an indicator to compute the numerical convergence of the simulations. Mesh 4 is used in this paper to conduct the simulations because the match between Mesh 4 (3,583,674 elements) and Mesh 5 (6,831,328) is within 0.3%; therefore, the differences in computed values are minimal. The parameters presented in Table 1 were used for the simulations. For the metabolic activity, we considered values of 5,000, 10,000, 29,000, 45,000 and 70,000 W/m³; these values cover the range of metabolic activities for tumors reported in [37]. Simulations were also conducted for a breast without tumor. Figure 5 shows the surface temperature distributions over the breast for all six cases considered. For a breast without tumor, the surface temperature is layered with the coldest region located near the nipple. This is expected as this region is the farthest from the chest wall. Then, the temperature increases in a layered pattern as the distance to the chest wall decreases as observed in [38]. For a tumor with a metabolic activity of 5,000 W/m³ (low activity tumor), the surface temperature and the layered pattern are distorted near the region of the tumor. In addition, a hot spot is visible, which indicates the presence of an abnormality within the breast. For a metabolic activity of 10,000 W/m³ (low to moderate), the local hot spot becomes larger. For higher metabolic activities, alterations in the surface temperature induced by the tumor become further evident.

Figure 6 shows the surface temperature profile obtained along a line passing through the center of the tumor projected on the surface. The temperature on a breast without tumor decreases almost linearly as the distance from the chest wall increases. In the presence of a tumor, the surface temperature in the vicinity of the tumor increases and reaches its maximum at the location of the tumor. To measure the temperature rise caused by the presence of the tumor, we compared each case with the corresponding temperature of a breast without tumor. The maximum temperature rise values for each metabolic activity simulated were 0.665° , 0.693° , 0.797° , 0.884° and 1.023° C for $q_m = 5,000$, 10,000, 29,000, 45,000 and 70,000 W/m³, respectively. From Figures 5 and 6, it can be seen that the temperature rise and the temperature distribution near the location of the tumor is different for each metabolic activity used. Thus it is seen that a careful examination of the surface temperature of the breast in prone position provides detectable thermal signature that is useful in the detection of breast cancer.

passing through the line in Figure 6. In a breast without tumor, the temperature pattern is layered and isotherm lines follow the outline of the breast. In the presence of a tumor, the heat generated by tumor metabolic activity is dissipated to the surrounding tissue, which causes deviation from the layered pattern. For low metabolic activities (5,000 and 10,000 W/m³), the temperature of the tumor remains lower than 37 °C and the warming effect of the tumor is confined only to the immediate surrounding tissue. For higher metabolic activities, the temperature of the tumor is higher than 37 °C and the warming

effect extends to a larger area within the breast. These temperature distributions agree with the findings reported in Figures 5 and 6.

4.3 – DISCUSSION

The results presented in this paper demonstrate the potential of the digital breast model developed using sequential MRI images to accurately determine the surface temperature distribution of a breast with and without tumor. The UDFs used in the thermal simulation software were validated by comparing the computed temperature profile with a hemispherical model data available in literature. This comparison provided confidence in the temperature predictions and the approach used.

Findings reported in this paper demonstrate that the temperature distribution can be correlated with the presence of a tumor. Further, it may provide estimates of the metabolic activity of the tumor (Figure 6). A detailed study of the effect of various tumor parameters such as size, position and metabolic activity on the surface temperature distribution is planned in future work.

5. – CONCLUSIONS

In this paper a digital model was generated for a female breast in prone position.

The model was developed from a sequence of MRI images of a breast with tumor; the approach resulted in a seamless and smooth digital model of the breast. This digital model was used to conduct numerical simulations with the Pennes bioheat equation in a

commercial CFD software ANSYS Fluent. The perfusion rate and metabolic activity terms in the Pennes bioheat equation were implemented by means of User Defined Functions (UDFs). Many previous works have not considered studying a breast in prone position and therefore detailed clinical data is unavailable. Therefore, we validated the ability of our UDF to predict the temperature distribution using a hemispherical model data available in literature. Simulations were conducted for six different cases, namely, a breast without tumor, and with a tumor experiencing metabolic activities ranging from 5,000 to 70,000 W/m³. In all the simulations with tumor, the tumor was located at a depth of 4.5 cm and the diameter of the tumor was 2.9 cm. Results from these simulations indicate a temperature rise on the breast surface of 0.665 °C for a metabolic activity of 5,000 W/m³. The temperature rise increased as the metabolic activity increased; the maximum temperature rise was 1.023 °C for a tumor with a metabolic activity of 70,000 W/m³. Results also indicated that the temperature profile can be correlated with the presence of a tumor and its metabolic activity.

FUNDING

This project was partially funded by the grant CBET 1640309 of the National Science Foundation.

CONFLICT OF INTERESTS

The authors have not conflict of interests to declare.

REFERENCES

- [1] R. L. Siegel, K. D. Miller, and A. Jemal, "Cancer statistics, 2016," *CA. Cancer J. Clin.*, vol. 66, no. 1, pp. 7–30, Jan. 2016.
- [2] "Breast Cancer Risk in American Women," *National Cancer Institute*. [Online]. Available: https://www.cancer.gov/types/breast/risk-fact-sheet. [Accessed: 14-Nov-2016].
- [3] "American Medical Association | AMA." [Online]. Available: https://www.ama-assn.org/. [Accessed: 10-May-2017].
- [4] "Final Update Summary: Breast Cancer: Screening US Preventive Services Task Force," 14-Nov-2016. [Online]. Available: https://www.uspreventiveservicestaskforce.org/Page/Document/UpdateSummaryFin al/breast-cancer-screening. [Accessed: 14-Nov-2016].
- [5] "Final Update Summary: Breast Cancer: Screening US Preventive Services Task Force." [Online]. Available: https://www.uspreventiveservicestaskforce.org/Page/Document/UpdateSummaryFin al/breast-cancer-screening. [Accessed: 14-Nov-2016].
- [6] S. A. Narod *et al.*, "Screening mammography and risk of breast cancer in BRCA1 and BRCA2 mutation carriers: a case-control study," *Lancet Oncol.*, vol. 7, no. 5, pp. 402–406, May 2006.
- [7] S. M. Friedewald *et al.*, "Breast Cancer Screening Using Tomosynthesis in Combination With Digital Mammography," *JAMA*, vol. 311, no. 24, p. 2499, Jun. 2014.
- [8] C. K. Kuhl *et al.*, "Mammography, Breast Ultrasound, and Magnetic Resonance Imaging for Surveillance of Women at High Familial Risk for Breast Cancer," *J. Clin. Oncol.*, vol. 23, no. 33, pp. 8469–8476, Nov. 2005.
- [9] B. B. Lahiri, S. Bagavathiappan, T. Jayakumar, and J. Philip, "Medical applications of infrared thermography: A review," *Infrared Phys. Technol.*, vol. 55, no. 4, pp. 221–235, Jul. 2012.
- [10] D. J. Watmough and R. Oliver, "Wavelength dependence of skin emissivity," *Phys. Med. Biol.*, vol. 14, no. 2, p. 201, 1969.
- [11] T. L. Bergman, F. P. Incropera, D. P. DeWitt, and A. S. Lavine, *Fundamentals of Heat and Mass Transfer*. John Wiley & Sons, 2011.
- [12] T. Yahara, T. Koga, S. Yoshida, S. Nakagawa, H. Deguchi, and K. Shirouzu, "Relationship Between Microvessel Density and Thermographic Hot Areas in Breast Cancer," *Surg. Today*, vol. 33, no. 4, pp. 243–248, Aug. 2016.
- [13] M. Gautherie, "Thermobiological assessment of benign and malignant breast diseases," *Am. J. Obstet. Gynecol.*, vol. 147, no. 8, pp. 861–869, Dec. 1983.
- [14] A. J. Guidi and S. J. Schnitt, "Angiogenesis in Preinvasive Lesions of the Breast," *Breast J.*, vol. 2, no. 6, pp. 364–369, Nov. 1996.
- [15] M. Gautherie and C. M. Gros, "Breast thermography and cancer risk prediction," *Cancer*, vol. 45, no. 1, pp. 51–56, Jan. 1980.
- [16] S. G. Kandlikar *et al.*, "Infrared imaging technology for breast cancer detection Current status, protocols and new directions," *Int. J. Heat Mass Transf.*, vol. 108, Part B, pp. 2303–2320, May 2017.

- [17] D. A. Kennedy, T. Lee, and D. Seely, "A Comparative Review of Thermography as a Breast Cancer Screening Technique," *Integr. Cancer Ther.*, vol. 8, no. 1, pp. 9–16, Mar. 2009.
- [18] L. A. Bezerra *et al.*, "Estimation of breast tumor thermal properties using infrared images," *Signal Process.*, vol. 93, no. 10, pp. 2851–2863, Oct. 2013.
- [19] H. H. Pennes, "Analysis of Tissue and Arterial Blood Temperatures in the Resting Human Forearm," *J. Appl. Physiol.*, vol. 85, no. 1, pp. 5–34, Jul. 1998.
- [20] M. Mital and R. M. Pidaparti, "Breast Tumor Simulation and Parameters Estimation Using Evolutionary Algorithms," *Model Simul Eng*, vol. 2008, pp. 4:1–4:6, Jan. 2008.
- [21] R. Hatwar and C. Herman, "Inverse method for quantitative characterisation of breast tumours from surface temperature data," *Int. J. Hyperthermia*, vol. 33, no. 7, pp. 741–757, Oct. 2017.
- [22] K. Das and S. C. Mishra, "Estimation of tumor characteristics in a breast tissue with known skin surface temperature," *J. Therm. Biol.*, vol. 38, no. 6, pp. 311–317, Aug. 2013.
- [23] A. Amri, S. H. Pulko, and A. J. Wilkinson, "Potentialities of steady-state and transient thermography in breast tumour depth detection: A numerical study," *Comput. Methods Programs Biomed.*, vol. 123, pp. 68–80, Jan. 2016.
- [24] M. M. Osman and E. M. Afify, "Thermal Modeling of the Normal Woman's Breast," *J. Biomech. Eng.*, vol. 106, no. 2, pp. 123–130, May 1984.
- [25] M. M. Osman and E. M. Afify, "Thermal Modeling of the Malignant Woman's Breast," *J. Biomech. Eng.*, vol. 110, no. 4, pp. 269–276, Nov. 1988.
- [26] N. M. SUDHARSAN, E. Y. K. NG, and S. L. TEH, "Surface Temperature Distribution of a Breast With and Without Tumour," *Comput. Methods Biomech. Biomed. Engin.*, vol. 2, no. 3, pp. 187–199, Jan. 1999.
- [27] N. M. Sudharsan and E. Y. K. Ng, "Parametric optimization for tumour identification: Bioheat equation using ANOVA and the Taguchi method," *Proc. Inst. Mech. Eng. [H]*, vol. 214, no. 5, pp. 505–512, May 2000.
- [28] F. J. González, "Thermal simulation of breast tumors," *Rev. Mex. Física*, vol. 53, no. 4, pp. 323–326, Aug. 2007.
- [29] N. M. S. E. Y. K. Ng, "Numerical computation as a tool to aid thermographic interpretation," *J. Med. Eng. Technol.*, vol. 25, no. 2, pp. 53–60, Jan. 2001.
- [30] E.-K. Ng and N. M. Sudharsan, "Effect of blood flow, tumour and cold stress in a female breast: A novel time-accurate computer simulation," *Proc. Inst. Mech. Eng. [H]*, vol. 215, no. 4, pp. 393–404, Apr. 2001.
- [31] L. Jiang, W. Zhan, and M. Loew, "Combined thermal and elastic modeling of the normal and tumorous breast," 2008, p. 69161E.
- [32] L. Jiang, W. Zhan, and M. H. Loew, "Modeling static and dynamic thermography of the human breast under elastic deformation," *Phys. Med. Biol.*, vol. 56, no. 1, p. 187, 2011.
- [33] J. Canny, "A Computational Approach to Edge Detection," *IEEE Trans. Pattern Anal. Mach. Intell.*, vol. PAMI-8, no. 6, pp. 679–698, Nov. 1986.
- [34] W. E. Lorensen and H. E. Cline, "Marching Cubes: A High Resolution 3D Surface Construction Algorithm," in *Proceedings of the 14th Annual Conference on*

- *Computer Graphics and Interactive Techniques*, New York, NY, USA, 1987, pp. 163–169.
- [35] R. Hess, *The Essential Blender: Guide to 3D Creation with the Open Source Suite Blender*. San Francisco, CA, USA: No Starch Press, 2007.
- [36] H. K. Versteeg and W. Malalasekera, *An introduction to computational fluid dynamics The finite volume method*. Pearson Education Limited.
- [37] M. Gautherie, "Thermopathology of Breast Cancer: Measurement and Analysis of in Vivo Temperature and Blood Flow," *Ann. N. Y. Acad. Sci.*, vol. 335, no. 1, pp. 383–415, Mar. 1980.
- [38] S. V. Francis, M. Sasikala, G. Bhavani Bharathi, and S. D. Jaipurkar, "Breast cancer detection in rotational thermography images using texture features," *Infrared Phys. Technol.*, vol. 67, no. Supplement C, pp. 490–496, Nov. 2014.
- [39] F. A. Duck, *Physical Properties of Tissues: A Comprehensive Reference Book.* Academic Press, 2013.
- [40] E. Y.-K. Ng, "A review of thermography as promising non-invasive detection modality for breast tumor," *Int. J. Therm. Sci.*, vol. 48, no. 5, pp. 849–859, May 2009.

Table Caption List

Table 1 Thermophysical properties and conditions used in the simulations.

Table 2 Grid independence study.

Figure Captions List

Fig. 1	Approach to generate breast geometry.
Fig. 2	Steps required to generate breast geometry in prone position
Fig. 3	Computational domain with the actual breast shape.
Fig. 4	Validation of the UDF with clinical data [37] using a hemispherical breast
	model.
Fig. 5	Surface temperature distribution for six cases with different tumor
	metabolic activities.
Fig. 6	Surface temperature profiles along centerline of tumor.
Fig. 7	Temperature distribution on a vertical plane passing though the tumor
	center.

Table 1. Thermophysical properties and conditions used in the simulations

Parameter	Value	Unit
Thermal conductivity (k) [37]	0.42	W m ⁻¹ K ⁻¹
Perfusion rate of healthy tissue (ω_h) [37]	1.8×10 ⁻⁴	S ⁻¹
Perfusion rate of tumor (ω_t) [37]	9×10 ⁻³	S ⁻¹
Metabolic activity of healthy tissue (q_h) [37]	450	W m ⁻³
Metabolic activity of tumor (q_t) [37]	5,000 -70,000	W m⁻³
Temperature of arteries (Ta) [39]	37	°C
Specific heat of blood (c_b) [39]	3,840	J kg ⁻¹ K ⁻¹
Density of blood (ρ_b) [39]	1,060	Kg m⁻³
Core temperature (T_c) [37]	37	°C
Ambient temperature (T_{∞}) [40]	21	°C
Heat transfer coefficient [24]	13.5	W m ⁻² K ⁻¹

Table 2. Grid independence study

Mesh number	Number of Elements	T _{max} (°C)	$\frac{T_{max}^{i+1} - T_{max}^i}{T_{max}^i} \times 100$
1	446,312	35.16	2.08
2	825,644	35.89	0.61
3	1,791,154	36.11	0.17
4	3,583,674	36.17	0.03
5	6,831,328	36.18	_

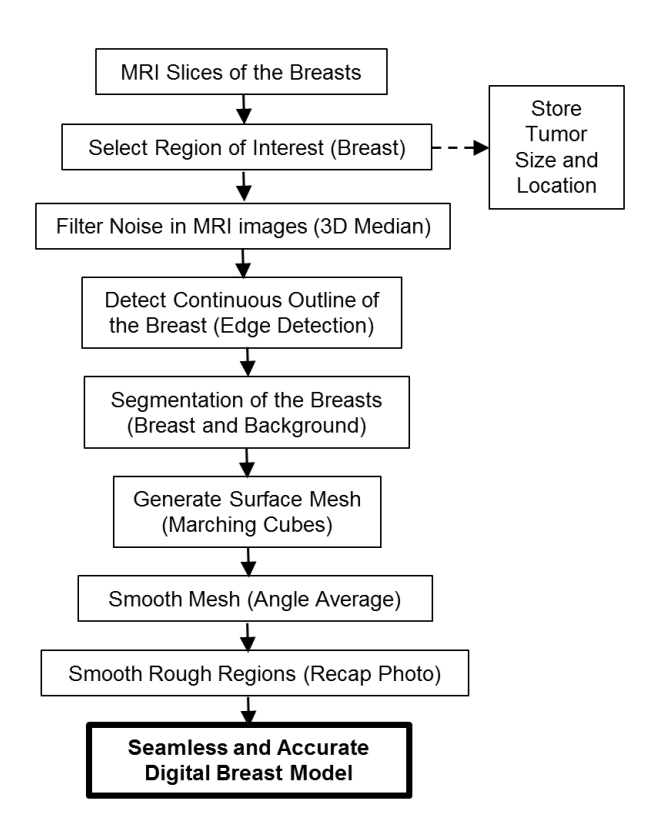


Figure 1. Approach to generate breast geometry.

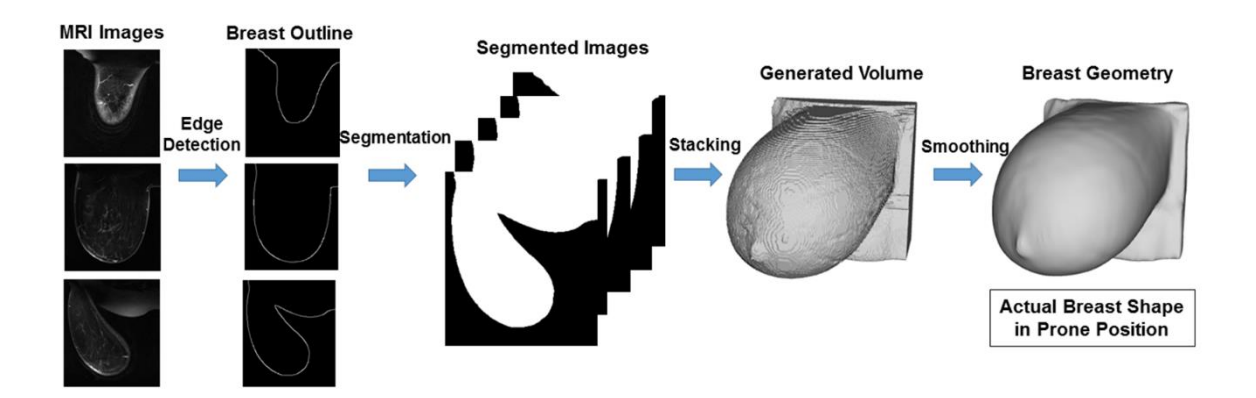


Figure 2. Steps required to generate breast geometry in prone position.

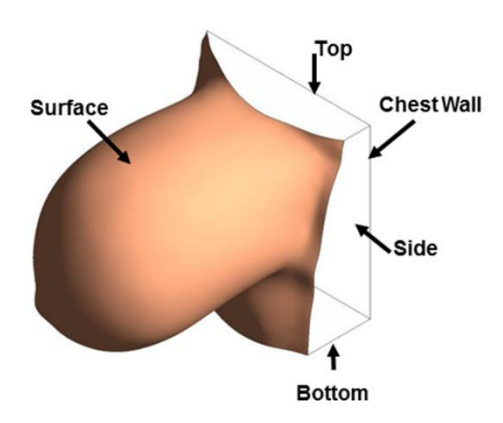


Figure 3. Computational domain with the actual breast shape.

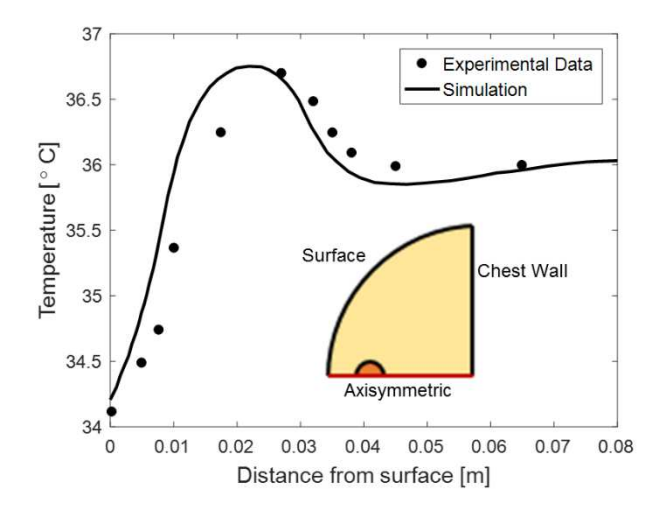


Figure 4. Validation of the UDF with clinical data [37] using a hemispherical breast model.

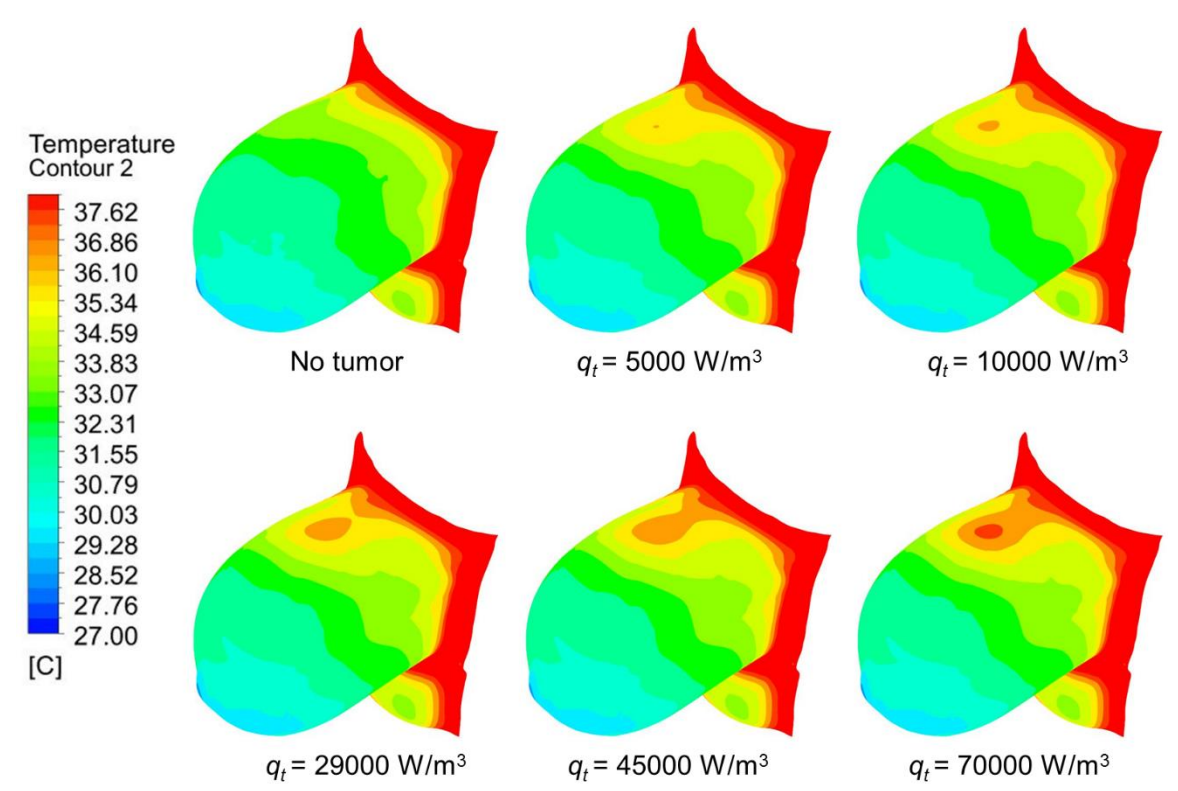


Figure 5. Surface temperature distribution for six cases with different tumor metabolic activities.

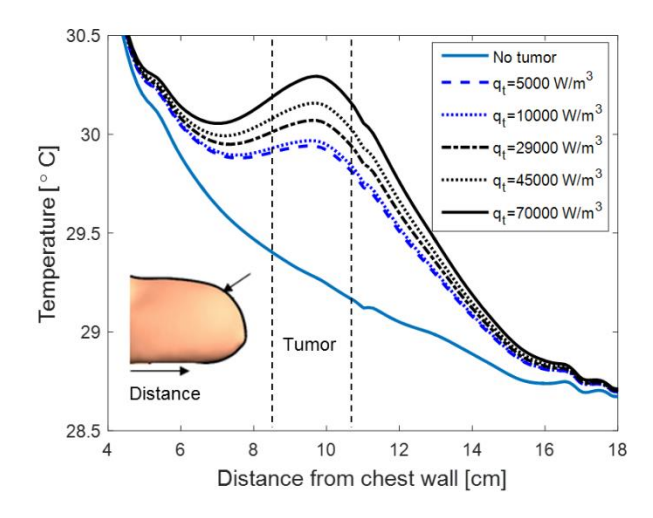


Figure 6. Surface temperature profile along centerline of tumor.

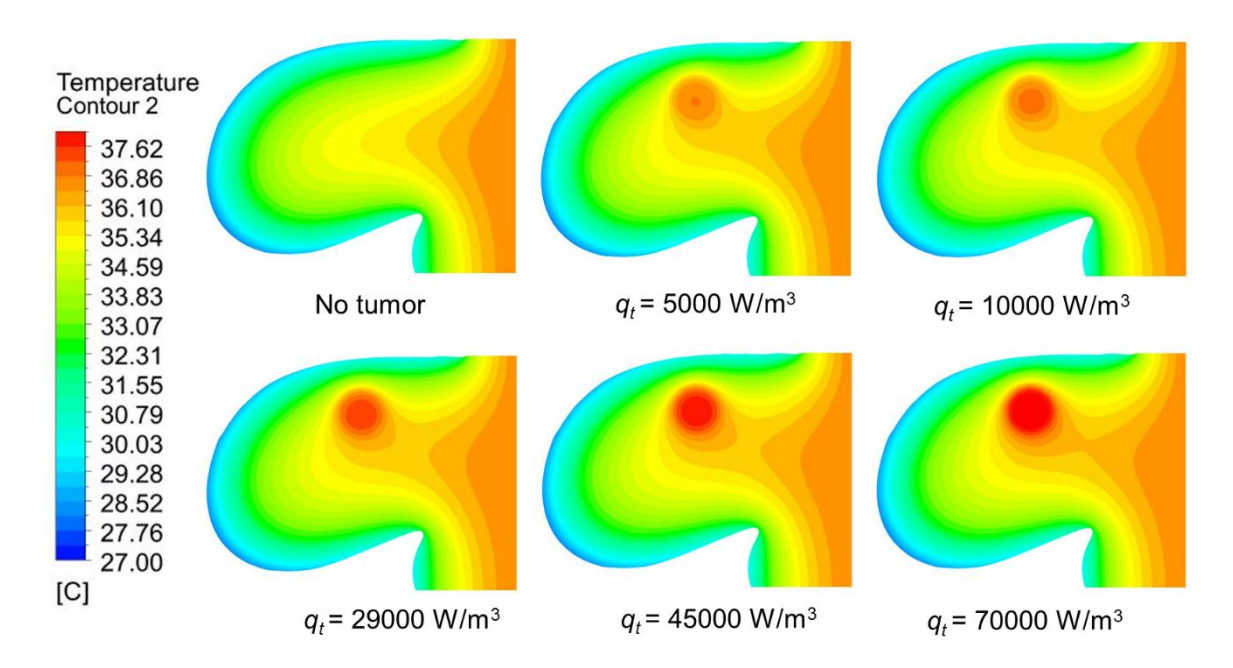


Figure 7. Temperature distribution on a vertical plane passing though the tumor center.